Roles of Laser Light and Heat in Formation of Single-Wall Carbon Nanotubes by Pulsed Laser Ablation of $C_xNi_yCo_y$ Targets at High Temperature

Masako Yudasaka,*,† Toshinari Ichihashi,‡ and Sumio Iijima†,‡

Nanotubulites Project, JST-ICORP, c/o NEC Corporation, 34 Miyukigaoka, Tsukuba 305-8501, Ibaraki, Japan, and NEC Corporation, 34 Miyukigaoka, Tsukuba 305-8501, Ibaraki, Japan

Received: August 4, 1998; In Final Form: October 6, 1998

Laser ablations were performed on $C_xNi_yCo_y$ targets (x, y = 98.8, 0.6 or 91, 4.5) using a Nd:YAG pulsed laser. Influences of the laser-beam intensity and atmospheric temperature on the structures of target surfaces and carbonaceous deposits were compared. These influences were found to be similar except for the following; the diameter did not change enormously when the laser-beam intensity was varied, while it decreased and its distribution range was widened as the atmospheric temperature decreased. The quantity of carbon expelled from the target was determined mainly by the laser-beam intensity, and the quantity of Ni and Co removed from the target was affected by both the laser-beam intensity and the atmospheric temperature. These results indicate that the atmospheric temperature controls the chemical reaction of carbon by which single-wall carbon nanotubes are formed, while the laser-beam intensity controls the process by which carbon, Ni, and Co are expelled from the target.

Introduction

The structure of the single-wall carbon nanotube (SWNT) was identified by Iijima in 1993.[1] Recently, high-yield formations of SWNTs by the laser-ablation method[2,3] and by the arc-discharge method[4] have been achieved. Methods of purifying SWNTs have been studied, and SWNTs almost completely free from non-SWNT carbon materials and metal catalysts have been produced.[5−7] As soon as these purification procedures were established, detailed studies on the chemistry[8] and physics[9−13] of the SWNT material could start. However, the formation mechanism of SWNTs is still open to question. The SWNT growth models proposed so far are sea-urchin (micrometer-scale metal-particle) growth,[14,15] one metal-atom catalyst growth,[16] and nanometer-scale metal-cluster catalyst growth.[2,17−19] We believe that clarifying the growth mechanism of SWNTs under laser ablation will extend our understanding of how the structure of carbon materials forms when the process is assisted by metal catalysts, and will be helpful in constructing custom-designed carbon materials.

To study the formation mechanism, the laser-ablation method is more preferable than the arc-discharge method because the number of experimental parameters controllable in the former is more than in the latter. For all that, mainly because of the high atmospheric temperature and transient phenomena with time scales that range from nanosecond to millisecond levels, in-situ observation of SWNT formation under laser ablation is diffult. Thus, as a substitute for in-situ observation, the structure of SWNTs have often been analyzed to infer the formation mechanism.[2,14,16,18,19] We have found that valuable information on the SWNT formation can be obtained through structure analysis of the target surface and non-SWNT carbon deposits, as well as of the SWNTs themselves. We took this approach in our recent study on the pressure dependence of the SWNT formation,[19] where we found that the pressure controls the laser-ablation rate of metal: the lower the pressure, the lower the ablation rate of metal, resulting in fewer SWNTs formed. In the research described in this report, we further considered the roles of the laser-beam intensity and the atmospheric temperature in the SWNT formation. Both of these provide energy to the reaction system, but the time scale and amount of energy greatly differ. When the SWNTs were formed, the laser-beam pulsed with a width of the nanosecond order elevated the target-surface temperature to 3000−4000 °C,[20,21] while the atmospheric temperature kept at a constant value between 600 and 1200 °C. We expected that these differences in the temperature and the time scale caused the two energy sources to play different roles in the formation process. In this research, we made the ranges of the laser-beam intensity and the atmospheric temperature as wide as possible to avoid misleading interpretation.

Experimental Section

The laser-ablation chamber was a quartz-glass tube with a length of 600 mm and a diameter of 37 mm. Each end of the quartz-glass tube had a quartz-glass window. The chamber was enclosed inside an electric furnace. The flow rate and pressure of Ar gas inside the chamber were 0.5 L/min and 600 Torr, respectively. An inner quartz-glass tube with a length of 50 mm and a diameter of 26 mm was located inside the chamber. A target was placed inside at the center of the inner quartz-glass tube. The atmospheric temperature around the target was raised by using the electric furnace.

The target was composed of carbon, Ni, and Co. The atomic percentage of the target was either 91:4.5:4.5 ($C_{91}Ni_{4.5}Co_{4.5}$) or 98.8:0.6:0.6 ($C_{98.8}Ni_{0.6}Co_{0.6}$). It was made by compressing a powder mixture of carbon, Ni, and Co into a disk with a diameter of 10 mm and a height of 5 mm. Diameters of the powder particles of carbon, Ni, and Co were about 5 μm.

A pulsed Nd:YAG laser beam (wavelength, 532 nm; pulse width, 6-7 ns; frequency, 10 Hz) irradiated the target surface perpendicularly for 60 s at a time.

* Corresponding author: E-mail: yudasaka@frl.cl.nec.co.jp.
† JST-ICORP.
‡ NEC Corp.

10.1021/jp983262k CCC: $15.00
Published on Web 11/17/1998

TABLE 1: Total Quantity of Spider-Web-Like Deposits (Q), Diameter (d) of SWNTs, Thickness (D_b) of SWNT Bundles, and quantity Ratio of SWNT and a-C (q_s/q_a) in the Spider-Web-Like Deposits and Quantity of Ni and Co (q_M) Remaining on the Target Surface, Size of C Clumps (D_C), and Quantity of a-C (q_{at}) on the Target Surface after the Laser Ablation[a,b]

	spider-web-like deposits[c]				targets		
	Q (web)	d (SWNT)	D_b (bundle)	q_s/q_a	q_M (Ni, Co)	D_c (C clump)	q_{at} (a-C)
	↑↓ [d]	→	→ or ↑	→	↑	↑	↑
I, ↑		(Fig. 1)	(Fig. 2 or Fig. 5)	(Figs. 2, 5)	(Fig. 3)	(Fig. 3)	(Fig. 4)
	↑	↑[f]	↑	↑	↓	→	→
T, ↑		(Fig. 6)	(Fig. 7)	(Fig. 7)	(Fig. 8)	(Fig. 8)	(Fig. 9)

[a] Q, d, D_b, q_s/q_a, q_m, D_c, and q_{at} all depend of laser-beam intensity (I) and atmospheric temperature (T). [b] ↑↓: increasing then decreasing (having a maximum). ↑: increasing. ↓: not changing. ↓: decreasing. [c] Powder deposits formed at 900 °C are included. [d] Detailed discussions are given in the last three paragraphs in the text and ref 19. [e] Detailed discussions are given in the text and ref 19. [f] Diameter distribution became wider as the temperature decreased.

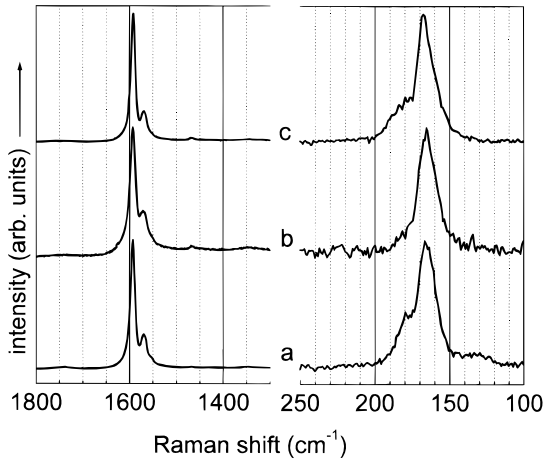

Figure 1. Raman spectra of spider-web-like deposits formed by laser ablation using $C_{91}Ni_{4.5}Co_{4.5}$ targets at laser-beam intensities of (a) 2, (b) 4, and (c) 6 (J/cm^2)/pulse.

To study the influence of the laser-beam intensity on the laser ablation, we kept the atmospheric temperature at 1200 °C. To study the influence of the atmospheric temperature, we kept the laser-beam intensity at 4 (J/cm^2)/pulse.

Results

Spider-web-like deposits were formed at the outlet of the inner quartz-glass tube when the laser-beam intensity was 2, 4, and 6 (J/cm^2)/pulse. The amount of these deposits formed when the intensity was 2 or 6 (J/cm^2)/pulse was about half or less of that formed when the intensity was 4 (J/cm^2)/pulse (Table 1). The Raman spectra of these deposits formed at 2, 4, and 6 (J/cm^2)/pulse (Figure 1) are similar; they exhibit peaks (at 165−168, 1569−1571, and 1591−1592 cm^{-1}) and shoulders (at 180−190 cm^{-1}). The peaks at 166−168 cm^{-1} have been reported to be due to the A_{1g} breathing mode of SWNTs with a diameter of 1.3 nm.[22] The shoulders at about 180−190 cm^{-1} are due to the A_{1g} breathing vibrations of SWNTs with diameters of about 1.2 nm.[13] We concluded from these Raman spectra (Figure 1) that the diameter distributions of the SWNTs formed when applying laser beams with different intensities of 2, 4, and 6 (J/cm^2)/pulse are similar (Table 1).

When the laser-beam intensity was either smaller (1 (J/cm^2)/pulse) or larger (8, 10, and 12 (J/cm^2)/pulse) than those values described above, the spider-web-like deposits were not formed at the outlet of the inner quartz-glass tube but film-like carbonaceous deposits appeared at the center of the inner quartz-glass tube in front of the target. The Raman spectra of these film-like deposits have only two broad peaks at around 1350 and 1600 cm^{-1}, indicating that they are amorphous carbon (a-C)[22] and do not contain SWNTs.

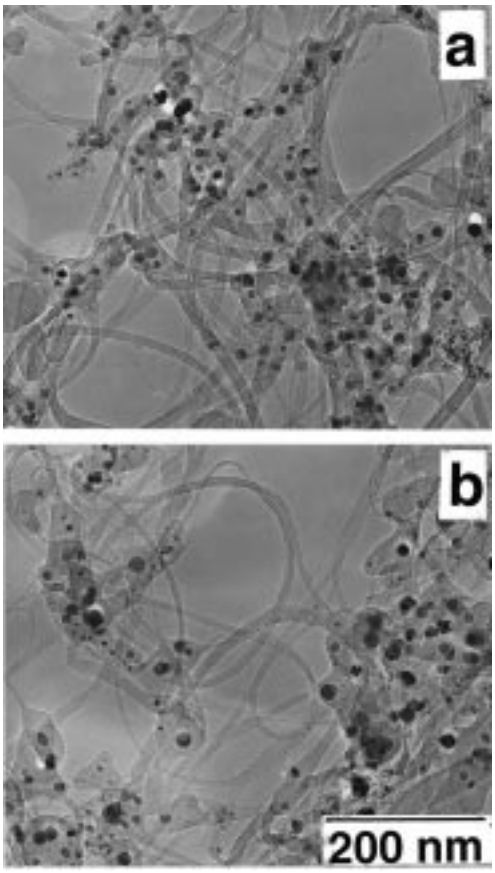

Figure 2. Transmission electron microscope images of spider-web-like deposits formed by laser ablation using $C_{91}Ni_{4.5}Co_{4.5}$ targets at laser-beam intensities of (a) 2 and (b) 6 (J/cm^2)/pulse.

Transmission electron microscope (TEM) images of the spider-web-like deposits obtained when the laser-beam intensity was 2 or 6 (J/cm^2)/pulse are shown in Figure 2. These two TEM images are similar in terms of the thickness of the bundles, quantity ratio of SWNTs and a-C particles (Table 1), and the size and amounts of the metal particles.

Scanning electron microscope (SEM) images of the laser-ablated surfaces of the targets (Figure 3) showed that the surface morphologies depended on the laser-beam intensity. The SEM image of the target surface laser-ablated with an intensity of 1 (J/cm^2)/pulse (Figure 3a) showed thin peaks (10−30 μm wide), many of which had metal caps. As the laser-beam intensity increased, the mountains became wider for 2 (J/cm^2)/pulse (Figure 3b), and large carbon clumps that were of 50−100 μm wide eventually appeared for 4 and 12 (J/cm^2)/pulse (Figure 3c,d) (Table 1). The coverage of Ni and Co metals over the carbon clumps when SWNT could be formed at 2 or 4 (J/cm^2)/pulse appeared to be similar (Figure 3b,c), while the coverage

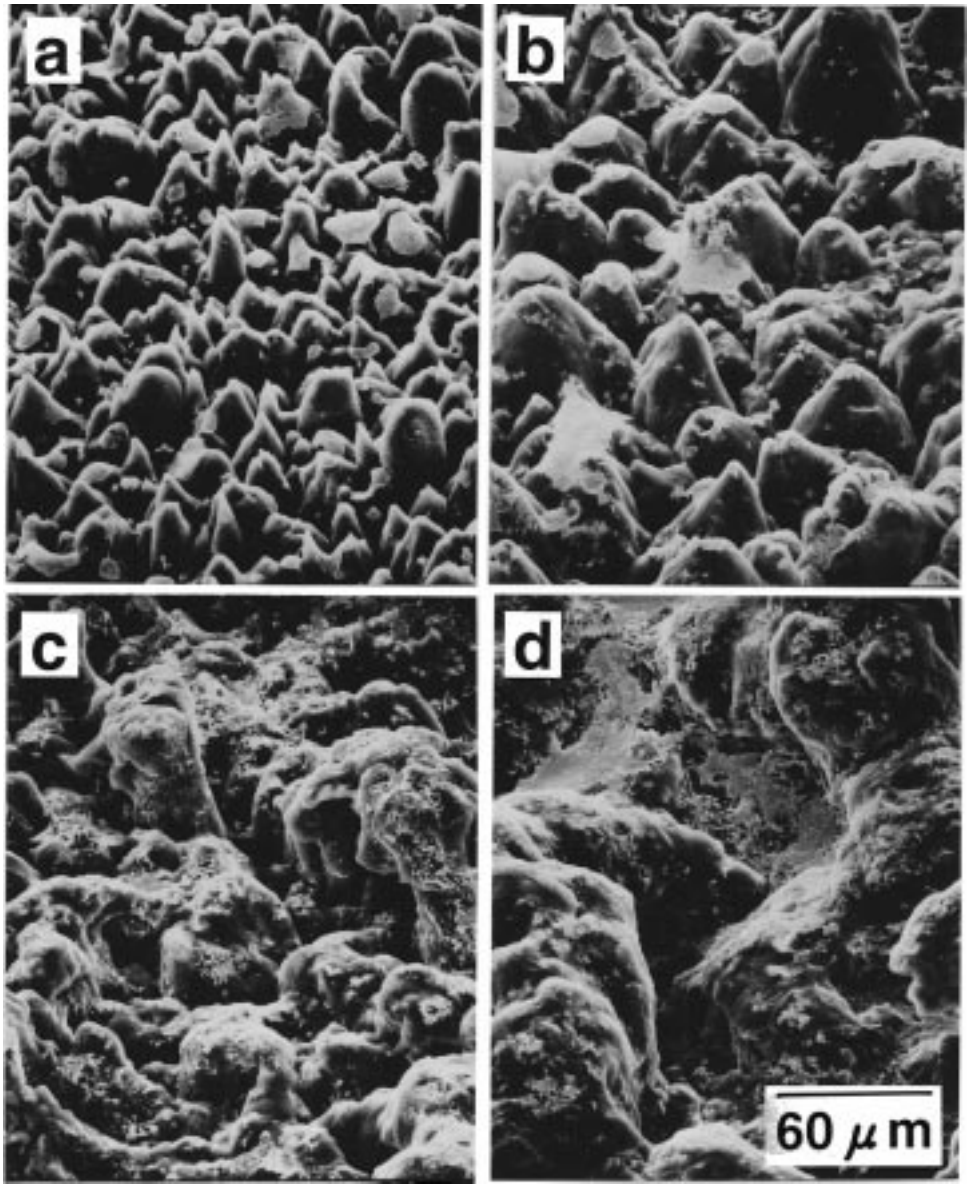

Figure 3. Scanning electron microscope images of $C_{91}Ni_{4.5}Co_{4.5}$ target surfaces laser-ablated at intensities of (a) 1, (b) 2, (c) 4, and (d) 12 (J/cm^2)/pulse.

apparently increased when the laser-beam intensity was increased to 12 (J/cm^2)/pulse (Figure 3d) (Table 1). (Elemental analysis using an x-ray microanalyzer indicated that the white areas in Figure 3 were mainly composed of Ni and Co metals, while the black or gray areas were mainly composed of C.)

The Raman spectra of the laser-ablated target surfaces also depended on the laser-beam intensity (Figure 4). The Raman spectrum of the initial target (Figure 4a) has a sharp peak at 1580 cm^{-1} and a small peak at 1360 cm^{-1}. These peaks are characteristic of graphite with small basal domain sizes.[22] The peak at around 1580 cm^{-1} in the spectrum for the target laser-ablated at 1 (J/cm^2)/pulse (Figure 4b) was somewhat broader. As the laser-beam intensity was further increased the two peaks became broader and the peak at 1360 cm^{-1} became stronger (Figure 4c−e). It is apparent from Figure 4 that the stronger the laser-beam intensity, the more the original graphite structure was decomposed, resulting in the appearance of a-C (Table 1).

The phenomena shown above did not depend on the initial concentration of Ni and Co in the target: We observed similar trends when we used the $C_{98.8}Ni_{0.6}Co_{0.6}$ target except for the following. The spider-web-like deposits were formed when the laser-beam intensity was above 2 (J/cm^2)/pulse, though their yield decreased when the laser-beam intensity exceeded 10 (J/cm^2)/pulse (Table 1). The TEM images showed that the bundles

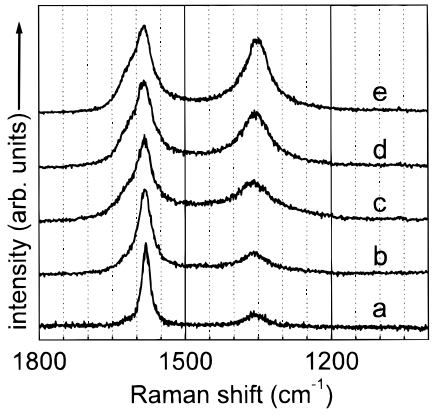

Figure 4. Raman spectra of $C_{91}Ni_{4.5}Co_{4.5}$ target surfaces (a) before laser ablation and after laser ablation at intensities of (b) 1, (c) 2, (d) 4, and (e) 6 (J/cm^2)/pulse.

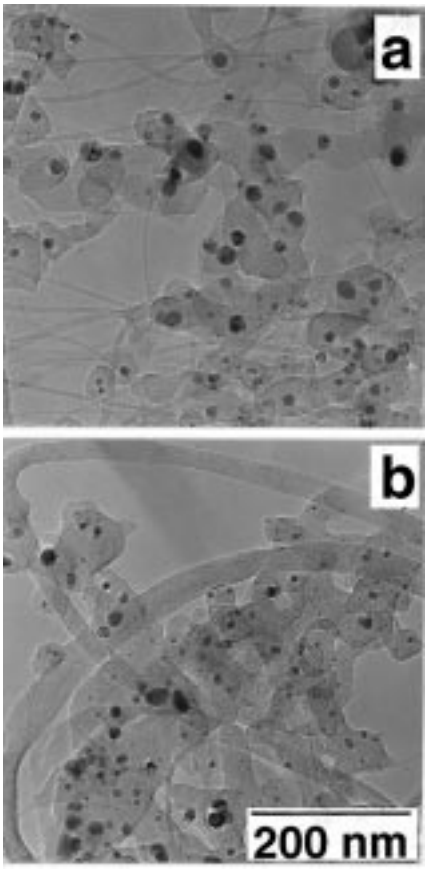

Figure 5. Transmission electron microscope images of spider-web-like deposits formed by laser ablation using $C_{98.8}Ni_{0.6}Co_{0.6}$ targets at laser-beam intensities of (a) 2 and (b) 10 (J/cm^2)/pulse.

became thicker as the laser-beam intensity increased (Figure 5) (Table 1). This is in contrast with the case of the $C_{91}Ni_{4.5}Co_{4.5}$ target where the bundle thickness did not depend on the laser-beam intensity (Figure 3). However, we believe that a similar laser-beam intensity dependence of the bundle thickness would also become apparent in the case of the $C_{91}Ni_{4.5}Co_{4.5}$ target if we could compare TEM images of SWNTs formed over as wide a range of laser-beam intensities.

The results described above indicate that the laser-beam intensity influenced the chemical structures of the carbon at the laser-ablated target surface, the morphology of the laser-ablated target surfaces, and the yields of SWNTs but changed the SWNT diameters only slightly (Table 1).

The influence of the atmospheric temperature on the quantities and structures of the spider-web-like deposits and target surfaces are shown below.

The spider-web-like deposits were obtained near the outlet of the inner quartz-glass tubes when the atmospheric temperatures were 1000, 1100, and 1200 °C. Its quantity decreased as the temperature decreased (Table 1). (The amount of the spider-web-like deposits at 1000 °C was less than 10% of that observed at 1200 °C.) At 900 °C, an extremely small quantity of powdery deposit was formed on the inside wall of the quartz-glass tube near its outlet (Table 1). The Raman spectra of the spider-web-like and powdery deposits (Figure 6) showed that the peak positions tended to shift to the higher wavenumber regions, that is, the diameter of SWNTs became narrower, as the temperature decreased (Table 1). (This is consistent with other recently reported results.[23,24] Peak positions and SWNT diameters estimated from the peak energy[13] are as follows. For 1200 °C (Figure 6d), the peak position was 166 cm^{-1} (the diameter is estimated to be 1.3 nm[13]). For 1100 °C (Figure 6c), the peak positions were 168 cm^{-1} (1.3 nm) and 185 cm^{-1} (1.2 nm). For 1000 °C (Figure 6b), they were 166 cm^{-1} (1.3 nm), 189 cm^{-1} (1.2 nm), and 205 cm^{-1} (1.1 nm). For 900 °C (Figure 6a), they were 177 cm^{-1} (1.25 nm) and 202 cm^{-1} (1.1 nm).

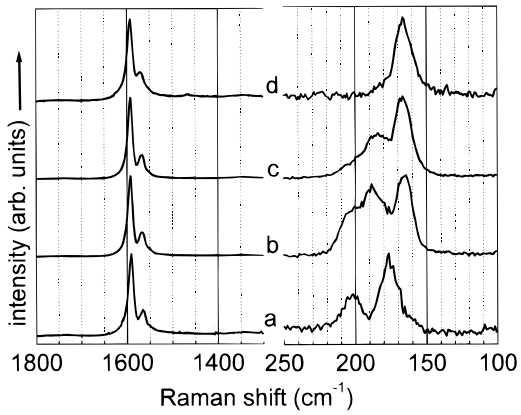

Figure 6. Raman spectra of spider-web-like deposits formed by laser ablation using $C_{91}Ni_{4.5}Co_{4.5}$ targets at atmospheric temperatures of (a) 900 °C, (b) 1000 °C, (c) 1100 °C, and (d) 1200 °C.

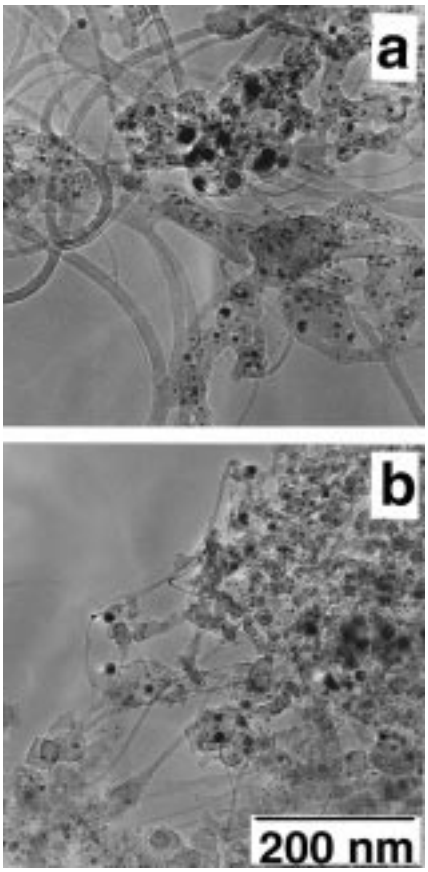

Figure 7. Transmission electron microscope images of spider-web-like deposits formed by laser ablation using $C_{91}Ni_{4.5}Co_{4.5}$ targets at atmospheric temperatures of (a) 900 °C and (b) 1000 °C.

The film-like deposits were formed in front of the target when the spider-web-like deposits were not formed at the outlet of the inner quartz-glass tube at temperatures of 900 °C or below. Their Raman spectra showed two broad peaks at around 1350 and 1600 cm^{-1}, indicating that they were a-C and did not contain SWNTs.

TEM images of the spider-web-like deposits indicated that the bundle thickness and the sizes and amounts of metal particles

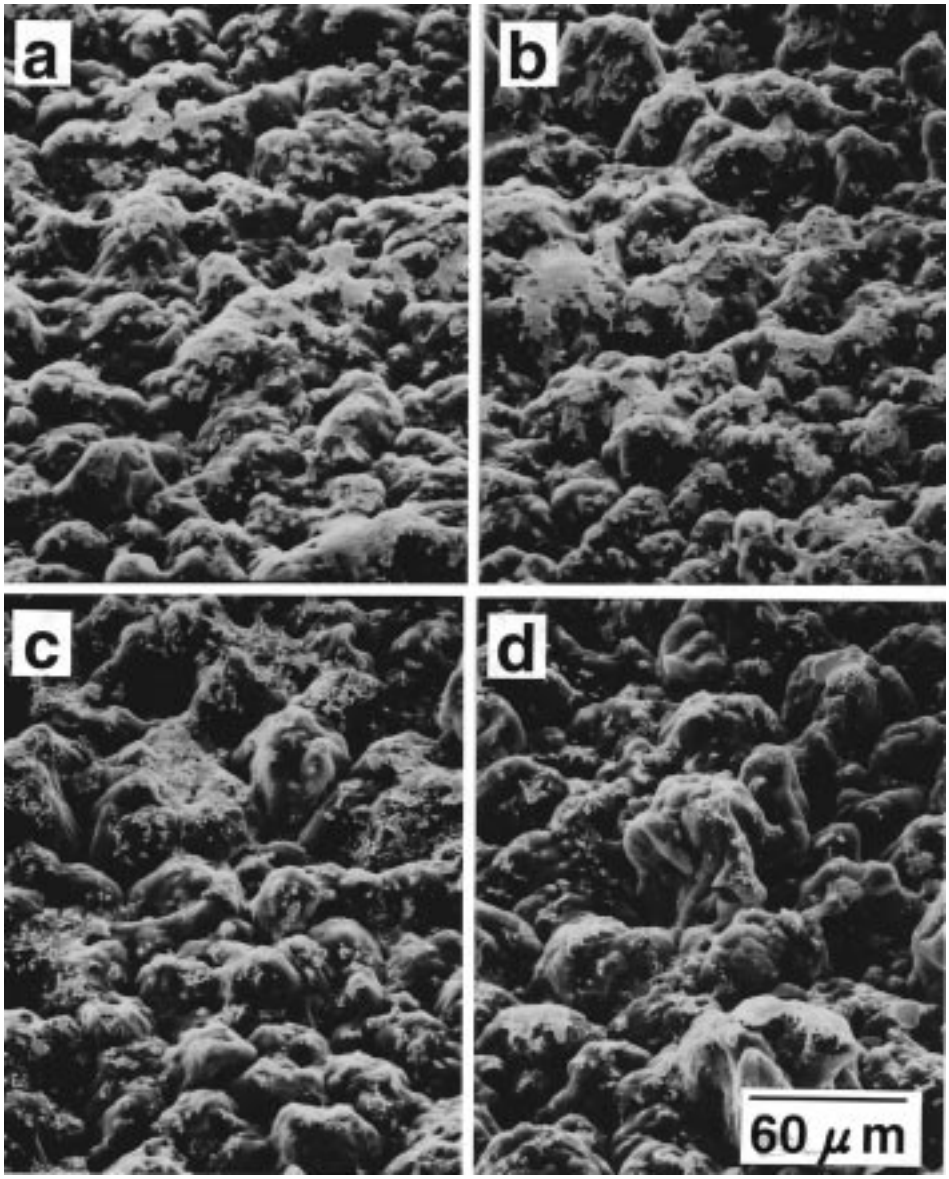

Figure 8. Scanning electron microscope images of $C_{91}Ni_{4.5}Co_{4.5}$ target surfaces laser-ablated at atmospheric temperatures of (a) 600 °C, (b) 900 °C, (c) 1000 °C, and (d) 1200 °C.

and a-C particles were similar for 1000 (Figure 7a), 1100, and 1200 °C. However, the bundle thickness was thinner, the amount of the metal particles was smaller, and there was more a-C when the temperature was 900 °C (Figure 7b) (Table 1).

SEM images of the laser-ablated targets (Figure 8) show that the sizes of the large dark clumps of carbon changed slightly when the atmospheric temperature was varied between 600 and 1200 °C. On the other hand, the amount of Ni and Co, which appear as a white covering on the carbon clumps, decreased obviously as the temperature decreased. These images show that the morphology of the carbon clumps is not very sensitive to the temperature, but the amount of metal removed from the target surface by the laser ablation decreases significantly as the temperature decreases (Table 1). This corresponds to the decrease of the metal-particle amount in the spider-web-like deposits (Figure 7) and the yield decrease of the spider-web-like deposits as the temperature decreases.

The Raman spectra of the laser-ablated targets (Figure 9) did not depend on the atmospheric temperature and showed the two broad peaks of a-C. Therefore, the decomposition of the graphite powder by the laser beam was not influenced by the atmospheric temperature (Table 1). This is consistent with the carbon clumps in the SEM images (Figure 8) not showing any temperature dependence.

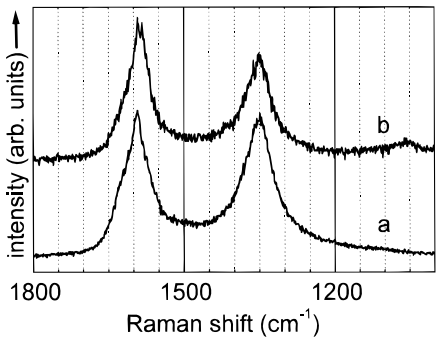

Figure 9. Raman spectra of $C_{91}Ni_{4.5}Co_{4.5}$ target surfaces laser-ablated at atmospheric temperatures of (a) 900 °C and (b) 1200 °C.

The influence of the temperature on the structures of the SWNTs and the target surfaces studied using the $C_{98.8}Ni_{0.6}Co_{0.6}$ target were similar to that for the target $C_{91}Ni_{4.5}Co_{4.5}$.

Comparing the influence of the laser-beam intensity and that of the atmospheric temperature on the SWNT formation (Table

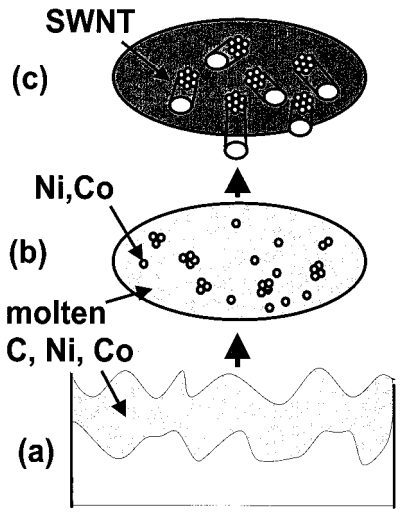

Figure 10. Formation mechanism of SWNT by laser ablation using $C_xNi_yCo_y$ target.

1) shows that the most remarkable differences are in the influences on the SWNT diameters (Figures 1 and 6) and carbon structures at the laser-ablated target surfaces (Figures 3, 4, 8, and 9). These differences indicate that the laser beam expels carbon and metal from the target surface to the Ar-gas atmosphere, and the high atmospheric temperature enables the chemical reaction of carbon to synthesize the SWNTs in the Ar-gas atmosphere assisted by Ni and Co catalysts.

Discussion

Before considering the temperature dependence of the SWNT diameter, we will briefly describe a model of SWNT formation by the ablation using the $C_xNi_yCo_y$ target that we previously proposed.[19] As the carbon at the target surface absorbs the laser-beam energy, its temperature rises to 3000−4000 °C and it melts.[20,21] The molten carbon makes a homogeneous solution with the Ni and Co (Figure 10a), and droplets of the C−Ni−Co mixture are expelled from the target surface (Figure 10b).[19] The mechanism of the droplets being expelled from the target is described in refs 25−27. (When the molten target surface is heated above the melting point by the pulsed laser-beam irradiation, the molten material vaporizes rapidly, resulting in the appearance of a recoil pressure on the molten material. This recoil pressure expels droplets of the molten materials from the target surface.) The C−Ni−Co droplets remain a homogeneous solution immediately after being expelled from the target (Figure 10b). As the droplets move away from the target though, they cool, and during this cooling, the metal atoms aggregate and form clusters (Figure 10c). When the cluster size reaches 1−2 nm, a metal cluster can act as a catalyst for the formation of an SWNT (Figure 10c), where the diameter of the cluster will determine the diameter of the SWNT.

This model can explain the temperature dependence of the SWNT diameter if we show that the metal-cluster size depends on the temperature as follows. The thermodynamic phase-diagrams of C−Ni and C−Co are similar, showing that solid C and solid Ni or Co that contains trace amounts of C segregate out of the C−Ni or C−Co solution at temperatures below about 1300 °C.[28] Since the Ni−Co phase diagram does not show any anomaly, we expect the C−Ni−Co system to behave similarly to the C−Ni and the C−Co systems. Referring to the C−Ni and C−Co phase diagrams, we can infer that the Ni and Co in the C−Ni−Co droplet start to segregate while continuing to contain a trace amount of C ((C−)Ni−Co) when the temperature of the droplet falls to about 1300 °C. If the atmospheric temperature is slightly lower than 1300 °C, the cooling rate of the droplets is slow, leading to the growth of large (C−)Ni−Co clusters. A slow cooling rate also narrows the cluster-size distribution. When the atmospheric temperature is much lower than the segregation temperature, the clusters become smaller and the size distribution becomes wider. This behavior corresponds to the dependence of the SWNT diameter on the atmospheric temperature (Figure 6). Thus, based on this model, we believe that the atmospheric-temperature dependence of the SWNT diameter can be explained by the temperature dependence of the sizes of the Ni−Co clusters and (C−)Ni−Co clusters. We also believe the (C−)Ni−Co cluster would catalyze the SWNT formation as the Ni−Co cluster does since the amount of carbon in the cluster is less than 3% according to the phase diagram.

The lack of any relationship between the atmospheric temperature and the chemical structure of carbon at the laser-ablated target surface (Figure 9) or its morphology (Figure 8), indicates that the temperature difference between 1200 and 600 °C does not affect the laser ablation of carbon where the target-surface temperature is raised to 3000−4000 °C.[20,21] The amount of metal expelled from the target depends on the atmospheric temperature (Figure 8), because it becomes easier for Ni and Co to make a solution with carbon when the atmospheric temperature (the initial target temperature) is close to the melting points of Ni (1455 °C) and Co (1492 °C). The decrease in the amount of expelled metal is the reason for the decreased quantity of SWNTs (Figures 6 and 7), the increased amount of a-C (Figure 7), and the bundle-thinning (Figure 7), as the atmospheric temperature decreases.

The laser-beam intensity influences the carbon chemical structure at the target surface, the quantity of carbon and metal expelled from the target surface, the quantity of SWNTs formed, and the bundle thickness. This can be explained straightforwardly without using the SWNT-formation model described above. As the laser-beam intensity rises, more energy is absorbed by the carbon, leading to a higher temperature and a faster ablation rate of the carbon. A higher temperature causes more Ni and Co to dissolve into the carbon melt, and droplets of a C−Ni−Co solution having a larger concentration of Ni and Co are expelled from the target. The higher metal concentration causes a higher yield of SWNTs, a lower yield of a-C, and the formation of thick SWNT bundles. (We have examined the influence of the amount of expelled metal on the bundle thickness in more detail in ref 19.)

This, however, does not explain the lower SWNT yield at higher laser-beam intensities, which became more evident when we used a target with a high metal concentration (Table 1). (This phenomenon has already been reported.[29]) The metal coverage of the target surface increases as the laser-beam intensity increases (Figure 3) because some of the metal is not expelled from the target and accumulates on the target surface. The rate of this accumulation is faster when the metal concentration is higher and the laser-beam intensity is stronger. As the metal coverage increases, the heat capacity of the metal clump rises and the exposure area of the carbon to the laser beam diminishes. As a result, the temperature of the C−Ni−Co mixture does not rise high enough for droplets to be expelled from the target surface. In this case, only carbon that does not mix with the metal would be expelled from the target, and this would form a-C.

Another effect of the laser-beam intensity on the target surface (Figure 3) is that the sharp carbon peaks change into large

rounded clumps as the laser-beam intensity increases. The reason for this is not discussed in detail here, but briefly we explain it as follows. The solid carbon is changed into a melt by the laser-beam irradiation as described above. This melt has a higher temperature as the beam intensity rises, resulting in higher fluidity and larger aggregations of carbon.

References and Notes

(1) Iijima, S.; Ichihashi, T. *Natyre* **1993**, *363*, 603.

(2) Guo, T.; Niklaev, P.; Thess, A.; Colbert, D. T.; Smalley, R. E. *Chem. Phys. Lett.* **1995**, *243*, 49.

(3) Thess, A.; Lee, R.; Nikolaev, P.; Dai, H.; Petit, P.; Robert, J.; Xu, C.; Lee, Y. H.; Kim, S. G.; Rinzler, A. G.; Tomanek, D.; Fisher, L. E.; Smalley, R. E. *Science* **1996**, *273*, 483.

(4) Journet, C.; Maser, W. K.; Bernier, P.; Loiseau, A.; Lamy, M.; de la Chapelle; Lefrant, S.; Deniard, P.; Lee, R.; Fisher, J. E. *Nature* **1997**, *388*, 756.

(5) Tohji, K.; Goto, T.; Takahashi, H.; Shinoda, Y.; Shimizu, N.; Jeyadevan, B.; Matsuoka, I.; Saito, Y.; Kasuya, A.; Ohsuna, T.; Hiraga, K.; Nishina, Y. *Nature* **1996**, *383*, 679.

(6) Tohji, K.; Takahashi, H.; Shinoda, Y.; Shimizu, N.; Jeyadevan, B.; Matsuoka, I.; Saito, Y.; Kasuya, A.; Ito, S.; Nishina, Y. *J. Phys. Chem. B* **1997**, *101*, 1874.

(7) Bandow, S.; Rao, A. M.; Williams, K. A.; Thess, A.; Smalley, R. E.; Eklund, P. C. *J. Phys. Chem. B* **1997**, *101*, 8839.

(8) Dillon, A. C.; Jones, K. M.; Bekkedahl, T. A.; Kiang, C. H.; Bethune, C. H.; Heben, M. J. *Nature* **1997**, *386*, 6623.

(9) Fisher, J. E.; Dai, H.; Thess, A.; Lee, R.; Hanjani, N. M.; Dehaas, D. L.; Smalley, R. E. *Phys. Rev. B, Condens. Matter* **1997**, *55*, 4921.

(10) Bockrath, M.; Cobden, D. H.; Mceuen, P. L.; Chopra, N. G.; Zettl, A.; Thess, A.; Smalley, R. E. *Science* **1997**, *275*, 1922.

(11) Maniwa, Y.; Sato, M.; Kume, K.; Kozlov, M. E.; Tokumoto, M. *Carbon* **1996**, *34*, 1287.

(12) Bandoh, S. *J. Appl. Phys.* **1996**, *80*, 1020.

(13) Rao, A. M.; Richter, E.; Bandoh, S.; Chase, B.; Eklund, P. C.; Williams, K. A.; Fang, S.; Subbaswamy, K. R.; Menon, M.; Thess, A.; Smalley, R. E.; Dresselhaus, G.; Dresselhaus, M. S. *Science* **1997**, *275*, 187.

(14) Ruoff, R. S.; Lorents, D. C.; Malhotra, R. *Nature* **1993**, *366*, 637.

(15) Maiti, A.; Brabec, C. J.; Bernholc, J. *Phys. Rev. B: Condens. Matter* **1997**, *55*, R6097.

(16) Kiang, C. H.; Goddard, W. A.; Beyers, R.; Salem, J. R.; Bethune, D. S. *Mater. Res. Soc. Symp. Proc.* **1995**, *359*, 69.

(17) Maiti, A.; Brabec, C. J.; Ronald, C.; Bernholc, J. *Phys. Rev., Condens. Matter.* **1995**, *52*, 14850.

(18) Fonseca, A.; Hernadi, K.; Piedigrosso, P.; Biro, L. P.; Lazarescu, S. D.; Lambin, Ph.; Thiry, P. A.; Bernaerts, D.; Nagy, J. B. *Proceedings of Fullerenes: Chemistry of Physics and New Directions IX*; The Electrochemistry Society Inc.: Montreal, 1997.

(19) Yudasaka, M.; Ichihashi, T.; Komatsu, T.; Iijima, S. *J. Phys. Chem. B* **1998**, *102*, 4892.

(20) Steinback, J.; Braunstein, G.; Dresselhaus, M. S.; Venkatesan, T.; Jacobson, D. C. *J. Appl. Phys.* **1988**, *58*, 4374.

(21) Achiba, Y. Private communication.

(22) Kinoshita, K. Carbon, *Electrochemical and Physicochemical Properties, 3*; John Wiley & Sons: New York, 1988; Chapter 2.2.

(23) Bandow, S.; Asaka, S.; Saito, Y.; Rao, A. M.; Grigorian, L.; Richter, E.; Eklund, P. C. *Phys. Rev. Lett.* **1998**, *80*, 3779.

(24) Kataura, Y.; Achiba, Y. Private communication.

(25) Baldwin, J. M. *J. Appl. Phys.* **1973**, *44*, 3362.

(26) Olstad, R. A.; Olader, D. R. *J. Appl. Phys.* **1975**, *46*, 1499.

(27) Cheung, J.; Horwitz, J. *MRS Bull.* **1992**, *18*, 30.

(28) Massalski, T. B. *Binary Alloy Phase Diagrams*; American Society for Metals; Metal Park, OH 44073, 1986.

(29) Yudasaka, M.; Komatsu, T.; Ichihashi, T.; Iijima, S. *Chem. Phys. Lett.* **1997**, *278*, 102.